LARGE EDDY SIMULATIONS OF TWO-DIMENSIONAL TURBULENT INCLINED PLUMES

Xinya YING[1], Juichiro AKIYAMA[2], Masaru URA[3]

[1] Student Member of JSCE, Doctorial Student, Dept. of Civil Engineering, Kyushu Institute of Technology (1-1 Sensuicho, Tobataku, Kitakyushu 804, Japan)
[2] Member of JSCE, Associated Professor, Dept. of Civil Engineering, Kyushu Institute of Technology
[3] Member of JSCE, Professor, Dept. of Civil Engineering, Kyushu Institute of Technology

The motions of starting plumes traveling down slopes are investigated by large eddy simulations. The formulation of the model is based on the filtered two-dimensional Navier-Stokes equations and transport equation for density excess which is deduced from the conservation of mass. The subgrid-scale turbulent stress is evaluated by the Smagorinsky model. It is found that the model can give a good description of the front of inclined plumes over a wide range of slope angle ($10° \leqq \theta \leqq 90°$), when the following empirical relationships for the Smagorinsky constant $Cs = 0.06 + 0.1 \sin\theta$ and for the subgrid turbulent Schmidt number $Scs = 0.4 - 0.3 \sin\theta$ are used. The computational results further revealed the flow pattern, the density distribution as well as the mechanism of entrainment at the head of inclined plumes.

***Key words** : density current , inclined, plume, LES, Smagorinsky model*

1. INTRODUCTION

When dense fluid is constantly released from the upstream end of a slope into a less dense environment, the dense fluid will move down along an incline and spread under the action of its own buoyancy force (see Fig.1). The motions of this form are often referred to as inclined plumes. The discharges of sediment-laden water or dense waste water into a reservoir or coastal seas are typical examples of inclined plumes. In order to understand their impact on environment, it is important to predict how suspended sediments or waste matter are dispersed.

A great deal of experimental and analytical studies on inclined plumes has been performed. For examples, Britter and Linden[1)] have studied the flows over the range of slopes $5° \leqq \theta \leqq 90°$ and found the dimensionless front propagation speed $U_f^* = U_f / (B_0 q_0)^{1/3} = 1.5 \pm 0.2$, where inflow buoyancy force $B_0 = g(\rho_0 - \rho_a)/\rho_a$, and q_0 is inflow rate. In addition, it is revealed that the rate of growth of the head height, dH/dx , and the aspect ratio of height to length of the head, H/L, are proportional to slope angle θ . Further studies on the inclined plumes over the range of slopes $5° \leqq \theta \leqq 90°$ have been performed by Akiyama et al.[2),3),4)] and more detailed and accurate information on the flows has been obtained. A mathematical model to predict such plume characteristics as front velocity, head height and density has been also developed.

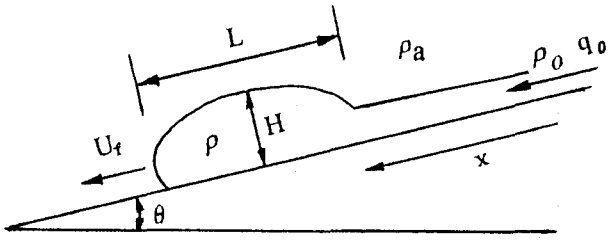

Fig.1 Definition sketch of an inclined plume

In the aspect of the numerical simulations of inclined plumes, only a few work is reported in literature. For example, Michioku et al.[5)] used the $k-\varepsilon$ model to simulate the flow on a slope of θ =5.71°, yet only made a few qualitative analyses on

the flow characteristics of the front of inclined plumes. To the authors' best knowledge, the systematic studies of inclined plumes using numerical simulations have not been reported in literature.

Herein the large eddy simulation (LES) is used to predict the flows. It is known that the large range scales exist in turbulent flows and the various scales make different contributions to the correlation terms. In addition, large scales can not be always considered as isotropic. These lead the large-scale-averaging approach for turbulent simulation is not always satisfactory. The direct numerical simulations (DNS), in which the whole range scales are computed by using very fine mesh, require considerable computation time and computer memory. The large eddy simulation is a promising approach to overcome these difficulties. In the large eddy simulation only the effect of small scales is modeled, while the large scales are directly computed. Since small scales tend to be more isotropic than the large ones, the modeling of them should be simpler and more universal than the large-scale-averaging approach.

Since Deardorff[6] had made his pioneer contribution in 1970, LES has been developed further by Yoshizawa[7),8)], Germano et al.[9)], Moin and Kim[10)], Piomelli et al.[11)], Horiuti[12)], Schumann[13)] and other researchers. Many encouraging results have been obtained and it has been shown that LES using simple models, such as the Smagorinsky model, can yield good predictions for various types of turbulent flows, including open channel flows, thermal convection, multiphase flows and so on.

In this study, the Smagorinsky model is employed to simulate inclined plumes. The detailed comparisons between computational and experimental results are made.

2. MODEL FORMULATION

In large eddy simulation, the large-scale quantities $F(\vec{r},t)$ (i.e. average values in local space) are defined by convolution of the physical variates $f(\vec{r},t)$ with a filter function $G(\vec{r},\vec{r}')$, where $\vec{r}$ is coordinate in space.

$$F(\vec{r},t)=\int_{\infty} G(\vec{r},\vec{r}')f(\vec{r}',t)d\vec{r}' \qquad (1)$$

By applying the grid filter to the two-dimensional incompressible Navier-Stokes equations and mass transport equation, ignoring Leonard and Cross terms, we can obtain the following governing equations.

$$\frac{\partial U_i}{\partial x_i}=0 \qquad (2)$$

$$\frac{\partial U_i}{\partial t}+U_j\frac{\partial U_i}{\partial x_j}=-\frac{1}{\rho}\frac{\partial P}{\partial x_i}+\nu\frac{\partial^2 U_i}{\partial x_j^2}+\frac{\partial}{\partial x_j}\left(-\overline{u_i'\ u_j'}\right)+g_i\frac{\Delta\rho}{\rho} \qquad (3)$$

$$\frac{\partial \Delta\rho}{\partial t}+U_i\frac{\partial \Delta\rho}{\partial x_i}=\frac{\partial}{\partial x_i}\left(-\overline{u_i'\ \Delta\rho'}\right) \qquad (4)$$

where U_i is the large-scale quantities of velocity component in the direction x_i; P is the large-scale pressure minus the hydrostatic pressure at reference density ρ_a; ρ is large-scale density ; $\Delta\rho$ is density excess, i.e. $\Delta\rho=\rho-\rho_a$; g_i is the specific body force in the direction x_i; u_i', $\Delta\rho'$ are fluctuating velocity and density excess. $\overline{u_i'\ u_j'}$ are correlation terms between fluctuating velocity due to space averaging. By using eddy viscosity concept, the correlation terms take the form

$$-\overline{u_i'u_j'}=\nu_t\left(\frac{\partial U_i}{\partial x_j}+\frac{\partial U_j}{\partial x_i}\right)-\frac{2}{3}k\delta_{ij} \qquad (5)$$

where ν_t is the subgrid scale eddy viscosity ; k is the turbulent kinetic energy ; δ_{ij} is the Kronecker delta function. The last term in Eq. (5) represents the normal stresses and can be absorbed in the pressure terms of the momentum equations.

In the Smagorinsky model, the eddy viscosity ν_t is obtained by assuming that turbulent energy production and dissipation of subgrid scale eddies are in balance. This leads following expression;

$$\nu_t=(Cs\Delta)^2\left|\overline{S}\right| \qquad (6)$$

where Δ is the filter width, $\left|\overline{S}\right|=\left(2\overline{S}_{ij}\overline{S}_{ij}\right)^{1/2}$ is the magnitude of large scale strain rate tensor

$$\overline{S}_{ij}=\frac{1}{2}\left(\frac{\partial U_i}{\partial x_j}+\frac{\partial U_j}{\partial x_i}\right) \qquad (7)$$

and Cs is the Smagorinsky constant. Many previous studies[14)] have shown the Smagorinsky constant needs some adjustments from flow to flow and the values vary from 0.07 to 0.27 for various flows. For examples, Lilly[15)] used Cs=0.23 for homogeneous isotropic turbulence; Deardorff[6)] used Cs=0.1 for turbulent channel flow; Piomelli et al.[11)] found the optimum value of Cs to be around 0.1.

$-\overline{u_i'\Delta\rho'}$ is generally assumed to be

$$-\overline{u_i'\Delta\rho'}=\frac{\nu_t}{Scs}\frac{\partial\Delta\rho}{\partial x_i} \qquad (8)$$

Tab.1 Computational conditions

θ °	B_0 (cm/s^2)	q_o (cm^2/s)	L_X (cm)	L_Y (cm)
10	9.80	3.34	350	50
20	9.80	2.16	250	60
30	9.80	2.16	250	80
45	9.80	2.02	250	80
60	9.80	2.02	250	100
70	9.80	2.02	250	110
80	9.80	2.00	250	120
90	9.80	2.00	250	120

* L_X and L_Y are the length and height of computational domain

where *Scs* is the subgrid turbulent Schmidt number and is defined as the ratio of eddy diffusivity of momentum to eddy diffusivity of matter. To the authors' best knowledge, so far the universal expression on the values of *Scs* has not been available. According to the studies by Reynolds[16], it can be assumed that turbulent Schmidt number bears perfect analogy with turbulent Prandtl number, the ratio of eddy diffusivity of momentum to eddy diffusivity of heat. Concerning subgrid turbulent Prandtl number *Prs*, Eidson[17] has indicated that it has different physical significance and does not equal to the value obtained for long-time-averaged turbulence. The studies by Eidson[17], Grotzbach[18] and Deardorff[17] suggest a range of *Prs*=1/2~1/3.

3. NUMERICAL SCHEME AND COMPUTATIONAL CONDITIONS

An operator-split algorithm is used to solve the governing equations. Diffusion terms in Eqs. (3) and (4) are discretized by central difference scheme. Advection terms are solved by the two-dimensional Hermitian interpolated pseudo-particle method, which has been found to be less diffusive and nearly free from numerical oscillation for the advection-diffusion problems[19),20]. The pressure is obtained by solving the Poisson type equation which is deduced from the algebraic manipulation of Eqs. (2) and (3).

The computational conditions are partially summarized in Tab.1. The computational region is a rectangle and the size is dependent on the slope angle θ, as shown in Tab.1. To verify the model, a wide range of slope angle θ is considered in the computation. Except inlet at upstream end and outlet at downstream end, other boundaries are considered as solid boundaries and no-slip boundary conditions are imposed. Grid size is 1cm $\times$ 1cm. The time interval ranges from 0.001 s to 0.1 s depending on the slope angle θ and the inflow buoyancy flux .

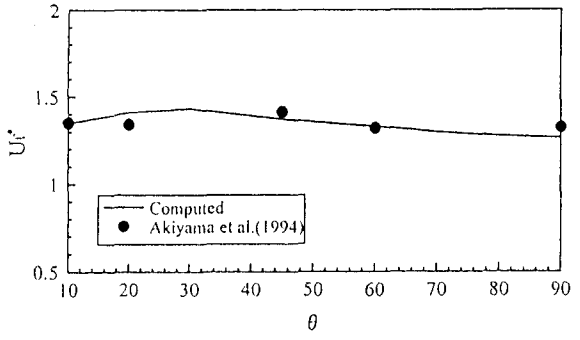

Fig.2 U_f^* as a function of θ
(B_0 and q_0 are shown in Tab.1)

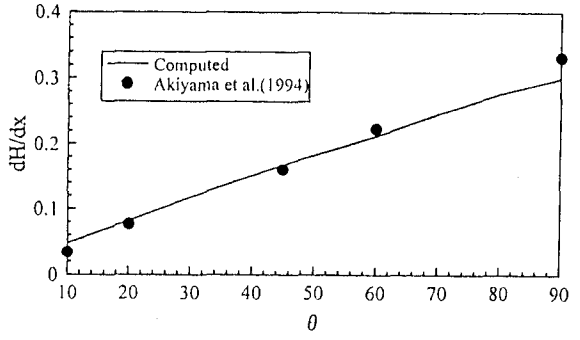

Fig.3 dH/dx as a function of θ
(B_0 and q_0 are shown in Tab.1)

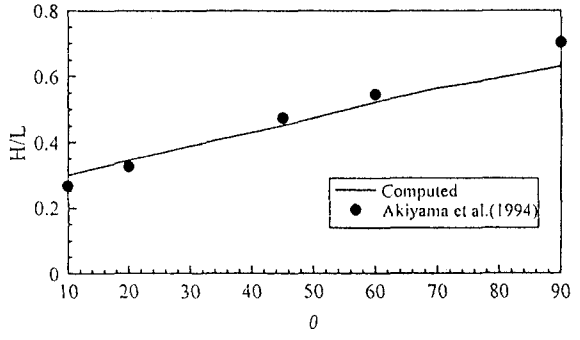

Fig.4 H/L as a function of θ
(B_0 and q_0 are shown in Tab.1)

4. THE COMPUTATIONAL RESULTS

In trial computations, it is found that the computational results are strongly dependent on the choice of the Smagorinsky constant *Cs* and the subgrid turbulent Schmidt number *Scs*. By the comparisons of main flow characteristics such as U_f^*, dH/dx and H/L between the computational results and experimental data obtained by Akiyama et al.[2] in the range of $10° \leqq \theta \leqq 90°$, we found the optimum value of *Cs* is a

function of θ and can be expressed as

$$Cs=0.06+0.1 \sin \theta \qquad (9)$$

Cs ranges from 0.077 to 0.16 for $10° \leqq \theta \leqq 90°$. Note that Cs ranges from 0.07 to 0.27 for various flows in previous studies[14]. Similarly, the optimum values of Scs can be expressed as

$$Scs=0.4-0.3 \sin \theta \qquad (10)$$

Note that in the cases of small slopes, the value of Scs given by Eq.(10) is within the range suggested in previous studies (see § 2).

The computed U_f^*, dH/dx and H/L by using the optimum values of Cs and Scs are compared with the experimental data in Figs. 2, 3 and 4, respectively. It is observed that the computational results can give good descriptions for all these flow characteristics of the front of inclined plumes. It should be noted that in the experiment the geometry of the front is rather difficult to be defined at θ =90°. This may cause some difference between computational results and experimental results observed in Figs.3 and 4.

In what follows, using the values of Cs and Scs estimated by Eqs.(9) and (10), the more detailed comparisons are made between experimental results and computational results.

(1) The comparisons between experimental and computational images

Fig.5 shows the experimental and the computational images of the flow on the slope θ =20°. In the figure the front is traveling from right to left. The region of plume in computational results is defined by $\Delta\rho/\rho_a \geq 10^{-5}$. It is seen that both are basically in agreement in shape, size and front velocity. In the experiment, it is observed that the flow at the wake of the head is quite unstable and part of dense clouds is left behind in the cases of small slope angle ($\theta \leqq 20°$). This phenomenon does not appear in the computation and it leads some difference between the experimental and the computational images. Because the density excess of left part is relatively small, it does not affect the motion of the front much. As the slope increases, the phenomenon also disappears in the experiment, and the experimental and the computational images seem to trend towards more consistent.

(2) Flow and density excess patterns

Fig. 6 shows computed typical flow and density excess patterns of the front for θ =10°, 45° and 80° at time=16 s. It is found that the head basically keep the shape of half-ellipse as described by

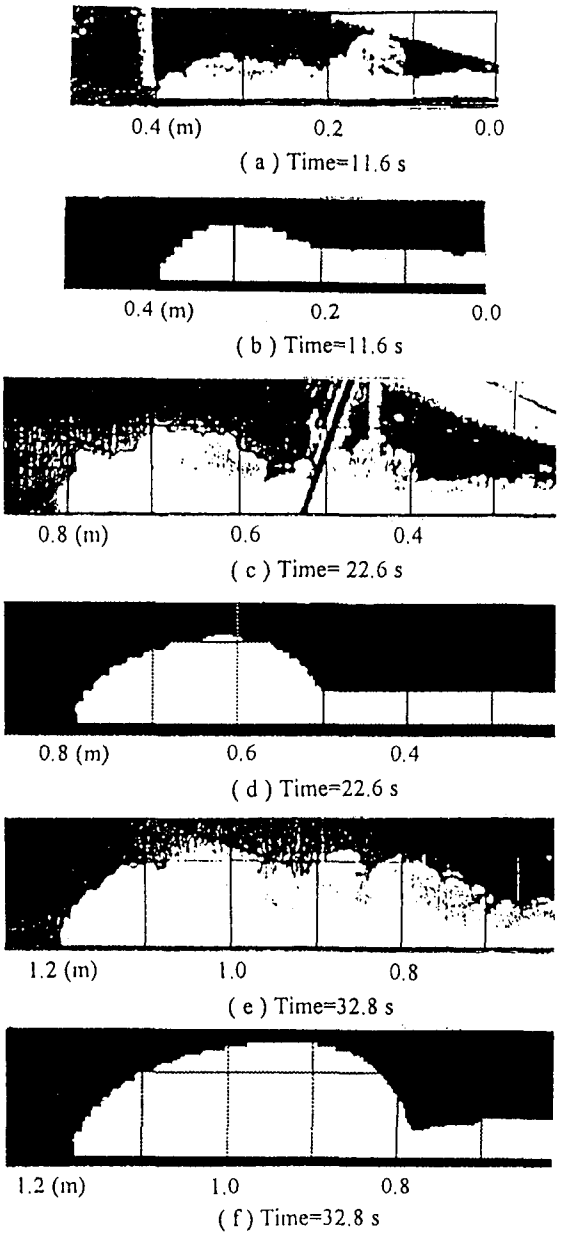

Fig.5 The experimental and the computational images for the front of θ =20° , B_0 =9.8 cm/s^2, q_0 =2.16 cm^2/s. (a), (c) and (e) are photographs from experiment. (b), (d) and (f) are computational images corresponding to (a), (c) and (e), respectively.

previous experimental studies[1),2)], and becomes larger as the slope increases. The flow pattern of the front is characterized by a large vortex motion centered near the top of the front. The vortex motion is weaker in the case of small slope and becomes stronger as the slope increases. By comparing these figures, we can find that the entrainment of ambient fluid at the rear of the front is weaker in the case of small slope angle and becomes stronger as the slope angle increases. This is a main reason why the head becomes larger as the slope increases.

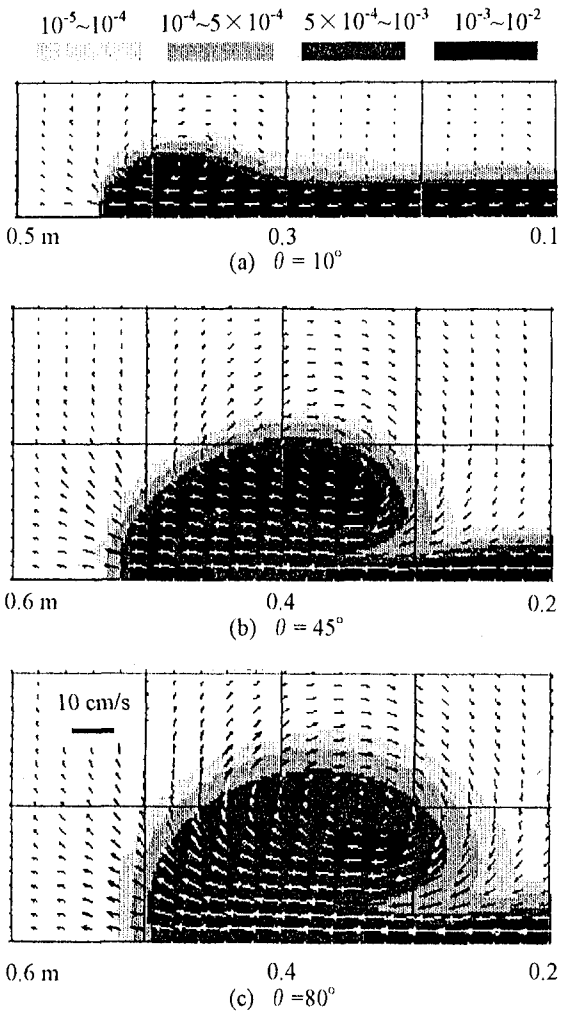

Fig.6 Velocity fields and density excess fields
(B_0 =9.8 cm/s^2, q_0 =2.0 cm^2/s)

Also there is some difference between the density excess fields for small slopes and for large slopes. In the cases of large slope such as $\theta = 45°$ and 80°, a peak of density excess appears at the place little lower than the center of the vortex motion, due to the stronger entrainment of fluid with less density from the rear of the front. For the case of $\theta = 10°$, the maximum of density excess always appears near the bottom.

(3) The constancy of U_f, dH/dx and H/L

For one case of $\theta = 45°$, the computed values of front propagation speed U_f , height of head H, and the aspect ratio of height to length H/L at different distance are examined in Figs.7, 8 and 9, in which the experimental data obtained by Akiyama, et al.[2] are also included. In these figures, x_f is the distance from inlet to the front position. We found that the experimental results fluctuate much stronger than the computational

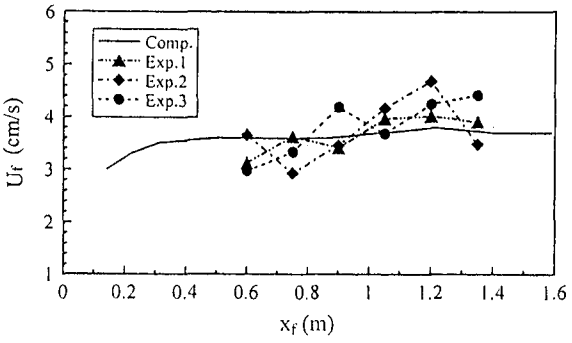

Fig.7 U_f as a function of distance ($\theta = 45°$)
(B_0 =9.8 cm/s^2, q_0 =2.02 cm^2/s)

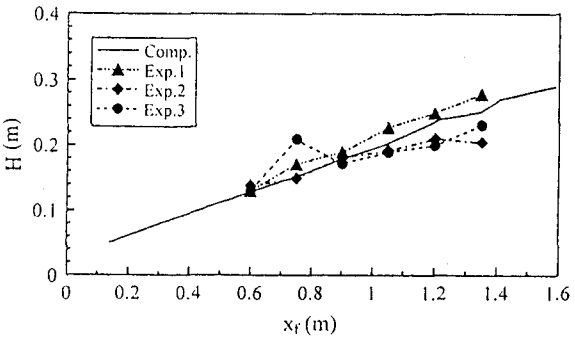

Fig.8 H as a function of distance ($\theta = 45°$)
(B_0 =9.8 cm/s^2, q_0 =2.02 cm^2/s)

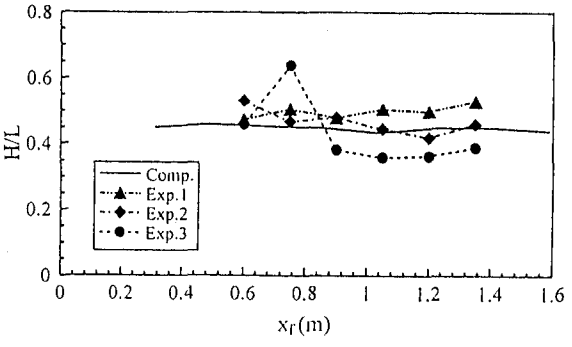

Fig.9 H / L as a function of distance ($\theta = 45°$)
(B_0 =9.8 cm/s^2, q_0 =2.02 cm^2/s)

results, but averagely both are in good agreement.

These figures also show that the values of U_f and H/L nearly keep constant after a certain distance, and H increases linearly as the head moves forward. This also means that U_f^* and dH/dx are nearly constant at different distance. It has been found these conclusions are still correct for the flows at other slope angle. However, it should be noted that there is some difference between the flow on large slope and small slope. The head for small slope such as θ =10° has a small acceleration than that for large slope, due to weak gravitational force in forward direction, so that it moves slower within a certain

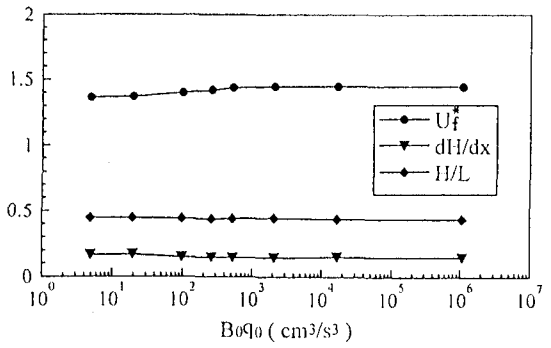

Fig.10 Computed U_f^*, dH/dx and H/L as a function of inflow buoyancy flux $B_0 q_0$ ($\theta = 45°$)

distance and needs a longer distance to reach a stable velocity.

(4) The effect of inflow buoyancy flux

The effect of inflow buoyancy flux $B_0 q_0$ on inclined plumes was examined experimentally by Britter & Linden[1] and Akiyama et al.[2] over a range of 2.5 $cm^3/s^3 \leq B_0 q_0 \leq 250$ cm^3/s^3. It is revealed that U_f^*, dH/dx and H/L are almost independent of $B_0 q_0$. For one case of $\theta = 45°$, the computed U_f^*, dH/dx and H/L by using the optimum values of Cs and Scs estimated by Eqs.(9) and (10), are plotted against $B_0 q_0$ in Fig.10 and no evident trend is found over a wide range of 4.95 $cm^3/s^3 \leq B_0 q_0 \leq 1.08 \times 10^6$ cm^3/s^3. The constancy of U_f^*, dH/dx and H/L against $B_0 q_0$ is also observed at other slope angles.

5. CONCLUSION AND DISCUSSION

The detailed comparisons between the computational results and the experimental data have shown that the model can give a good description for the front of inclined plumes over a wide range of slope ($10° \leqq \theta \leqq 90°$) and regardless of inflow buoyancy flux, when the Cs and Scs are calculated by the following empirical formulas $Cs = 0.06 + 0.1 \sin\theta$ and $Scs = 0.4 - 0.3 \sin\theta$. The computational results further revealed the mechanism of the internal flow and density distribution as well as entrainment at the head of inclined plumes.

As a means of comparison, we have used the one-equation model[12] to simulate the flow. In the one-equation model, the subgrid scale eddy viscosity ν_t is a function of turbulent kinetic energy, which is determined by solving the transport equation for turbulent kinetic energy. However, no apparent improvement over the Smogrinsky model is made. On the other hand, the Smogrinsky model is superior to the one-equation model in the following two aspects: (1) requires less computation time without solving turbulent kinetic equation; (2) needs to determine the constant C_s only.

For inclined plumes, excessive accuracy is required in solving the governing equation for density excess, since there is an interaction between density and flow. In addition, a steep density distribution often leads a solution with numerical oscillation and diffusion. The computational results show that this model is successful to overcome these difficulties by using Hermitian interpolated pseudo-particle scheme in solving the governing equation.

REFERENCE

1) Britter, R. E. and Linden, P. F.: *J. Fluid Mech.*, Vol. 99, pp. 531-545, 1980.
2) Akiyama, J., Ura, M.and Sakamoto, K.: *J. of Hydroscience and Hydraulic Engineering*, Vol.12, No.2, pp. 1-16, 1994
3) Akiyama, J., Ura, M. and Wongsa, S.: *J. of Hydroscience and Hydraulic Engineering*, Vol.12, No.2, pp. 17-30, 1994
4) Akiyama, J., Ura, M. and Wang, W.: *J. of Hydraulic Engineering*, ASCE, Vol.120, No.10, pp.1139-1158, 1994
5) Michioku, K., Fujikawa, Y. and Fuji, H.: *Proceedings of Hydraulic Engineering*, JSCE, Vol.40, pp.561-566, 1996, (in Japanese)
6) Deardorff J. W.: *J. Fluid Mech.*, Vol.41, pp.453-480,1970
7) Yoshizawa, A.: *Phys. Fluids* A 1 (7), pp.1293-1295, 1989
8) Yoshizawa, A.: *Phys. Fluids* A 3 (8), pp.2007-2009, 1991
9) Germano, M., Piomelli,U. and Cabot, W.H.: *Phys. Fluids* A 3 (7), pp.1760-1765, 1991
10) Moin, P. and Kim, J.: *J. Fluid Mech.*, Vol.118, pp.341-377, 1982
11) Piomelli, U., Moin, P., and Ferziger, J. H.: *Phys. Fluids*, Vol.31, pp.1884-1891, 1988
12) Horiuti K.: *J. of the Physical Society of Japan*, Vol.54, No.8, pp.2855-2865, 1985
13) Schumann, U.: *J. Comp. Phys.*, Vol.18, pp.376-404, 1975
14) Miyake, Y. and Kajishima, T.: *Proceedings of JSME* (B), JSME, Vol.53, No.491, pp.1869-1877, 1987, (in Japanese)
15) Lilly, D.K.: NCAR Manuscript No.123, 1966
16) Reynolds, A. J.: *Int. J. Heat Mass Transfer*, Vol. 18, pp. 1055-1069, 1975
17) Eidson, T. M.: *J. Fluid Mech.*, Vol. 158, pp.245-268, 1985
18) Grotzbach, G.: *Int. J. Heat Mass Transfer*, Vol. 24, pp. 457-490, 1980
19) H.Takewaki, T. Yabe, *J. Comp. Phys.*, Vol.70, pp.355-372, 1987
20) Ying,X.,Y.,Akiyama,J., Ura,M., The combined cubic spline method for advection-diffusion equation, to be submitted to JHHE

(Received September 30, 1997)